CHEMISTRY OF MATERIALS

Article

pubs.acs.org/cm

Influence of Compensating Defect Formation on the Doping Efficiency and Thermoelectric Properties of $Cu_{2-y}Se_{1-x}Br_x$

Tristan W. Day,[†,#] Kai S. Weldert,[‡,§,#] Wolfgang G. Zeier,[∥] Bor-Rong Chen,[∥] Stephanie L. Moffitt,[∥] Ulrike Weis,[⊥] Klaus P. Jochum,[⊥] Martin Panthöfer,[‡] Michael J. Bedzyk,[∥] G. Jeffrey Snyder,*[,†,∥] and Wolfgang Tremel*[,‡]

[†]Department of Applied Physics and Material Science, California Institute of Technology, Pasadena, California 91125, United States

[‡]Institut für Anorganische Chemie und Analytische Chemie der Johannes Gutenberg-Universität, Duesbergweg 10-14, D-55128 Mainz, Germany

[§]Graduate School Materials Science in Mainz, Johannes Gutenberg-Universität, Staudingerweg 9, 55128 Mainz, Germany

[∥]Department of Materials Science and Engineering, Northwestern University, Evanston, Illinois 60208, United States

[⊥]Biogeochemistry Department, Max Planck Institute for Chemistry, P.O. Box 3060, D-55020 Mainz, Germany

Supporting Information

ABSTRACT: The superionic conductor $Cu_{2-\delta}Se$ has been shown to be a promising thermoelectric at higher temperatures because of very low lattice thermal conductivities, attributed to the liquid-like mobility of copper ions in the superionic phase. In this work, we present the potential of copper selenide to achieve a high figure of merit at room temperature, if the intrinsically high hole carrier concentration can be reduced. Using bromine as a dopant, we show that reducing the charge carrier concentration in $Cu_{2-\delta}Se$ is in fact possible. Furthermore, we provide profound insight into the complex defect chemistry of bromine doped $Cu_{2-\delta}Se$ via various analytical methods and investigate the consequential influences on the thermoelectric transport properties. Here, we show, for the first time, the effect of copper vacancy formation as compensating defects when moving the Fermi level closer to the valence band edge. These compensating defects provide an explanation for the often seen doping inefficiencies in thermoelectrics via defect chemistry and guide further progress in the development of new thermoelectric materials.

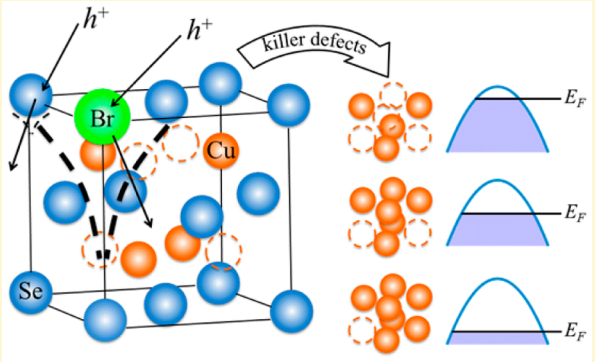

INTRODUCTION

On the basis of Seebeck and Peltier effects, thermoelectric materials either convert thermal to electrical energy or vice versa, providing a perspective for power generation and refrigeration applications, respectively. The thermoelectric efficiency is governed by the thermoelectric figure of merit $zT = S^2(\rho\kappa)^{-1}T$,[1,2] and the past decade has seen the discovery of many suitable materials for high temperature power generation. One of these materials is $Cu_{2-\delta}Se$, which exhibits a maximum zT of 1.6 at 1000 K, making it a competitive and cheap alternative for PbTe, the leading thermoelectric material in the hundreds of kelvin temperature range.[3] Because of a small, intrinsic copper deficiency δ, copper selenide ($Cu_{2-\delta}Se$) is a p-type semiconductor with a band gap of 1.23 eV.[4] Above 410 K, copper selenide transforms to a Cu^+ conducting phase, wherein the copper ions are mobile and described as "liquid like" because their diffusion coefficient is about 10^{-5} cm^2s^{-1}, comparable to the value for water molecules in liquid water.[5,6] This superionic state results in extremely low lattice thermal conductivity values as low as 0.4 $W(Km)^{-1}$ in the superionic phase and in turn a high figure of merit. Starting with the superionic $Cu_{2-\delta}Se$, many other superionic copper and silver selenides have been found to be interesting thermoelectrics; for instance, the argyrodites Cu_7PSe_6,[7] Ag_2Se,[8−10] CuAgSe,[11,12] and quaternary copper chalcogenides $Cu_2MM'Q_4$ (M = Zn, Fe,...; M′ = Zn, Ge, Q = S, Se, Te) which also exhibit interstitial copper ions and even show band convergence.[13−15] While copper selenide has potential as a thermoelectric material at high temperatures, its ionic conductivity has caused long-term stability problems for use in thermoelectric generators.[16] This spurs interest in the properties of copper selenide below the superionic phase transition at 410 K, where the ion migration would not be of concern. In this work, we investigate the potential for copper selenide to achieve high zT values at room temperature. Using bromine as a dopant, we show the effect of carrier scattering on the thermoelectric quality factor and how the dopant bromine itself prevents possibly high figures of merit at room temperature. Furthermore, we explore the

Received: June 24, 2015
Revised: September 24, 2015
Published: September 24, 2015

DOI: 10.1021/acs.chemmater.5b02405
Chem. Mater. 2015, 27, 7018−7027

underlying principle for doping inefficiencies in copper selenides via the intrinsic defect chemistry of this material. We show that doping not only introduces carriers into a semiconductor but also changes the overall stoichiometry of the host material. In the case of $Cu_{2-\delta}Se$, substitution of Se with Br introduces compensating defects in the form of additional Cu vacancies, which effectively pin the Fermi level and lead to a lower doping efficiency. In the following sections, the notation $Cu_{2-y}Se_{1-x}Br_x$ with $y > \delta$ will be used to take account of the additional defects in the Br doped samples.

EXPERIMENTAL SECTION

Synthesis. Bulk samples of polycrystalline $Cu_{2-y}Se_{1-x}Br_x$ with $x = 0$, 0.02, 0.03, 0.04, and 0.05 were prepared by melting and annealing techniques using powders of Cu (Alfa Aesar, 99.999%) and Se (Alfa Aesar, 99.999%), as well as CuBr (Sigma, 99.999%). In order to ensure the absence of copper oxides in the reaction mixture, the copper powder was reduced for several hours at 525 K under N_2/H_2 (95:5) flow in a tube furnace using a corundum boat as the reaction vessel. Phase purity of the starting materials was verified via X-ray diffraction, and all synthetic procedures were carried out in a N_2 drybox. The synthesis was performed in evacuated quartz ampules, which were dried at 1073 K under dynamic vacuum for several hours before usage. For the synthesis of $Cu_{2-y}Se_{1-x}Br_x$, the starting elements were thoroughly ground, sealed in quartz ampules, and heated to 1423 K for 1 h, then cooled down to 1073 K and annealed for 48 h. All procedures were carried out in box furnaces with heating and cooling rates of 5 K/min. Each mixture of starting materials had the nominal composition of $Cu_{2-y}Se_{1-x}Br_x$. However, after the annealing step, a small amount of unreacted elementary copper could be removed from the reaction product, indicating that the synthesized samples are slightly copper deficient (Supporting Information, Figure S7).[17,18] The obtained powders were hand ground and consolidated into 1−1.5 mm thick, 12 mm diameter discs at 873 K for 5 h under a pressure of 40 MPa by induction hot pressing in high density graphite dies.[19] The resulting pellets have more than 95% theoretical density, determined from the geometric densities.

Characterization. X-ray diffraction experiments were performed on a Siemens D5000 powder diffractometer equipped with a Braun M50 position-sensitive detector, Ge (111) monochromator (Huber 615 002), and Cu K_α radiation, with a step size of 0.0078°. Pawley fits were performed with TOPAS Academic V5.0 applying the fundamental parameter approach.[20] An exemplary diffraction pattern including the fit can be found in Figure S1. The photoelectron spectra (XPS) were collected on pressed pellets with a Thermo Scientific ESCALAB 250Xi with monochromatic Al K_α X-ray (1486.74 eV) and energy resolution of 0.42 eV. The surface was sputtered by a 3 keV electron gun for 120 s in order to remove the surface oxide layer prior to taking the measurement. The oxygen 1s peaks of both samples were completely removed after sputtering (Figure S3a). The carbon 1s peak (binding energy 284.5 eV) was used as a reference to calibrate the binding energies of the other core level spectra (Figure S3b). The relative contents of Cu to Se were determined using a Thermo-Finnigan ELEMENT2 single collector sector field-inductively coupled plasma mass spectrometer (ICP-MS). Information about sample preparation and operating parameters are given in the Supporting Information. X-ray Fluorescence (XRF) measurements were performed on an 18 kW rotating anode, two-circle diffractometer with monochromated Mo K_α radiation (E = 17.4 keV) operating at 50 kV and 160 mA. Spectra were taken at an incident angle of θ = 20°, resulting in an average penetration depth of 9.3 μm. The horizontal by vertical beam footprint at the sample was 0.6 × 6.3 mm, and the total collection time for each sample was 6 min. XRF data were collected with a Vortex-EM 350 μm thick silicon drift detector. The fluorescence yield was corrected for self-absorption and detector efficiency. Measured spectra can be found in Figure S4. The thermal diffusivity α was measured with a Netzsch laser flash diffusivity instrument (LFA 457) under continuous argon flow. In order to maximize the emissivity, samples were spray-coated with a thin layer of graphite before the measurement. Thermal conductivity was determined via $\kappa = \alpha C_p d$ with the heat capacity C_p and the geometric density d. C_p values from previous publications were used, which are in good agreement with the Dulong-Petit approximation up to 600 K, and a C_p independent of the Br content was assumed.[5,21] Electrical transport was characterized via measurements of the Seebeck coefficient, Hall coefficient, and electrical resistivity. Electrical resistivity and Hall coefficients were measured simultaneously using the van der Pauw technique with pressure-assisted contacts under dynamic vacuum. The Seebeck coefficient was calculated from the slope of the voltage versus temperature gradient measurements from chromel-Nb thermocouples under dynamic vacuum with a maximum ΔT of 7.5 K for all temperatures. Speed-of-sound measurements were performed at room temperature to extract the longitudinal and transverse sound velocities, respectively. The data were obtained by use of a Panametrics NDT 5800 pulser/receiver head; the response was recorded with a Tektronix TDS 1012 digital oscilloscope. Honey was used as a couplant between the sample and the ultrasonic transducer.

RESULTS AND DISCUSSION

Chemical Characterization. Copper selenide has a wide range of stoichiometric deviation ($Cu_{2-\delta}Se$).[17,22,23] Above 410 K, the compound has an average cubic structure with Se ions forming a face centered cubic lattice and copper ions being distributed over tetrahedral and trigonal sites.[24] The room temperature phase shows a very complex superstructure.[25] Several structures were proposed in the last decades and controversially discussed.[27−30] X-ray powder diffraction data of the synthesized samples are shown in Figure 1. Position and

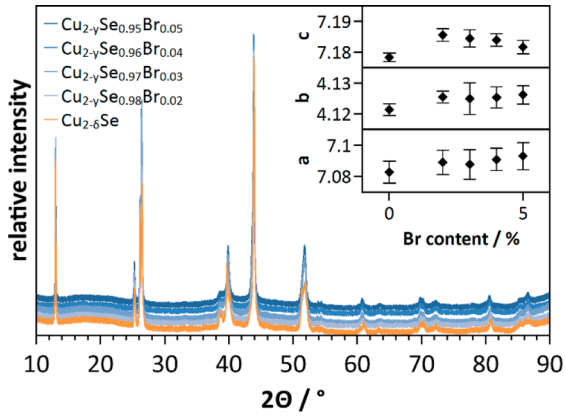

Figure 1. Room temperature X-ray powder diffraction data of the synthesized $Cu_{2-y}Se_{1-x}Brx$ with the formal composition $Cu_{2-y}Se_{1-x}Br_x$ (x = 0.00, 0.02, 0.03, 0.04, and 0.05). A triclinic anorthic unit cell derived from LP search (TOPAS Academic 4.1) was used in order to determine lattice parameters by Pawley fits for each composition. An exemplary Pawley fit of the Br-free sample can be found in Figure S1. Lattice parameters show no significant changes with composition; nevertheless, the obtained data are in very good agreement with literature diffraction data of $Cu_{2-\delta}Se$. No reflections of starting materials or possible impurity phases could be observed.

intensity of the observed reflections fit well to other experimental data of copper selenide in the literature.[31−33] Rietveld refinements against standard laboratory X-ray powder diffraction data with the published structure models do not provide reasonable information on positions or site occupancies. Se^{2-} and Br^- cannot be distinguished by X-ray diffraction techniques due to their similar atomic scattering form factors for X-rays. However, lattice parameters were derived from Pawley fits using a small, anorthic unit cell derived from a LP

DOI: 10.1021/acs.chemmater.5b02405
Chem. Mater. 2015, 27, 7018−7027

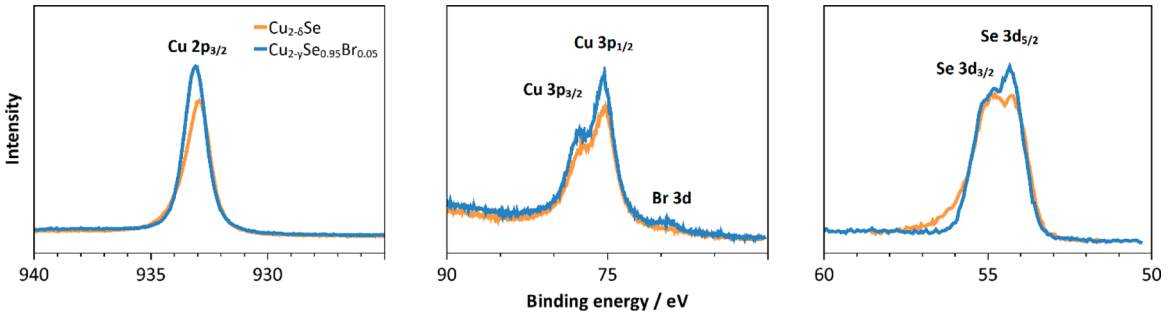

Figure 2. XPS core level spectra of $Cu_{2-\delta}Se$ (orange) and nominal $Cu_{2-y}Se_{0.95}Br_{0.05}$ (blue). After sputtering, only intensities from copper and selenium can be observed in the undoped sample and additionally bromine in the Br-doped sample. Compared with standard CuO and Cu_2O spectra, there are no features of oxidation in the investigated samples.[26] In combination with the diffraction data, the samples can therefore be considered as phase pure. Comparing doped and undoped samples directly, we can observe slight changes in peak position and peak shape, indicating that the local bonding environment might be slightly different in the investigated samples.

search (TOPAS Academic 5.0). Lattice parameters for the different compositions do not vary significantly nor do these values display a trend upon increasing bromide concentration, as can be expected from the similar ionic radii of Se and Br. The standard-laboratory X-ray powder diffraction data provide a hint that no secondary phases are present, as there are no signs of remaining starting materials or other crystalline secondary phases; however, it does not fully corroborate the extent of formation of a solid solution for the substitution of Se with Br. To check for (a) Br incorporation, (b) possible CuBr impurity phases, and/or (c) differences in the oxidation states resulting from impurity phases, X-ray photoemission spectroscopy (XPS) was used on pellets of the nominal compositions $Cu_{2-\delta}Se$ and $Cu_{2-y}Se_{0.95}Br_{0.05}$. Comparing the measured XPS spectra (Figure 2) of the sputtered $Cu_{2-\delta}Se$ sample with previously reported XPS data,[34,35] neither significant differences in peak position and peak shape nor additional peaks can be observed, indicating that no side phases or other oxidation states are present in the sample. A t higher values of x (x > 0.07), CuBr as secondary phases could be observed via X-ray powder diffraction (Figure S2), and these compositions were not analyzed in order to ensure that no phase segregation influences the transport.[36] For copper selenides, this is particularly important because they exhibit low carrier mobilities, and an impurity phase with high mobility would dominate the transport.[37] The presence of bromide ions in the doped sample can also be verified, as the corresponding 3d peak can only be seen in the doped sample. In addition, a shoulder on the high binding energy side can be observed in the Cu $2p^{3/2}$ and Se 3d peaks in the undoped but not in the doped sample. The account for the shoulder is not entirely clear, but it might be due to slight variations of the local bonding environment in the undoped sample. Since Br^- is expected to be an n-type dopant (electron donor), additional analysis with respect to the exact composition and the Br content is highly important in order to understand the thermoelectric transport properties. X-ray fluorescence (XRF) analyses were utilized in order to obtain the exact ratios of bromine to selenium in each sample. Because of an additional Cu signal in the XRF spectra from the sample holder, the relative Cu−Se composition cannot be extracted via XRF, and relative changes in the copper to selenium ratios were obtained using inductively coupled plasma mass spectroscopy (ICP-MS). Assuming that the undoped sample has the nominal composition of Cu_2Se, the changes in the stoichiometry of the doped samples can be calculated and are shown in Figure 3

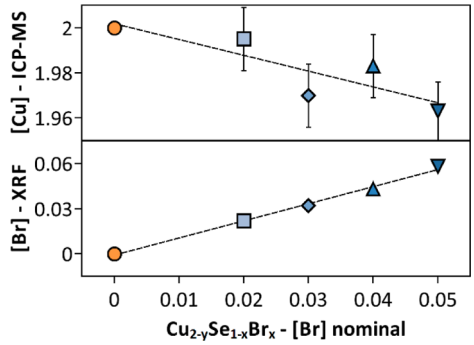

Figure 3. Composition of $Cu_{2-y}Se_{1-x}Br_x$ with the relative changes in the copper content [Cu] determined using ICP-MS and the Br content [Br] determined by X-ray fluorescence analyses. With increasing Br substitution for Se, the Cu content in the matrix decreases as well, leading to a larger Cu nonstoichiometry. Error bars in the ICP-MS analyses represent the standard error, and the error bars in the XRF analyses are smaller than the symbols.

and Table S1. First of all, these data show an increasing amount of bromide ions in the samples with increasing synthetic content. While the absolute values are slightly higher than expected, this shows the stoichiometric incorporation of Br for Se. Using the ICP-MS data, the relative amount of copper with respect to selenium and bromine decreases with increasing bromine concentration. In other words, with the increasing substitution of Se with xBr in $Cu_{2-y}Se_{1-x}Br_x$, the amount of Cu decreases as well, leading to a larger Cu nonstoichiometry as already observed for the undoped $Cu_{2-\delta}Se$ ($y > \delta$).[17,18] Therefore, y is influenced by both the intrinsic Cu non-stoichiometry of δ in $Cu_{2-\delta}Se$ and the change in x. As the absolute value of δ is small and there is a wide range of stoichiometric deviation in $Cu_{2-\delta}Se$, all compositions determined for $Cu_{2-y}Se_{1-x}Br_x$ are regarded with respect to Cu_2Se (δ = 0) in Figure 3. Here, the relative changes in the Cu content show that when two bromide ions are substituted for two selenium ions, the material becomes more deficient of roughly one Cu ion. The occurrence of this interesting defect chemistry and its influence on the thermoelectric transport will be discussed below.

Potential for High *zT* at Room Temperature in $Cu_{2-\delta}Se$. Figure 4a shows the temperature dependence of the measured zT values of different copper selenide samples with a nominal composition of $Cu_{2-\delta}Se$. However, a significant variation of the measured transport can be observed, which is

DOI: 10.1021/acs.chemmater.5b02405
Chem. Mater. 2015, 27, 7018−7027

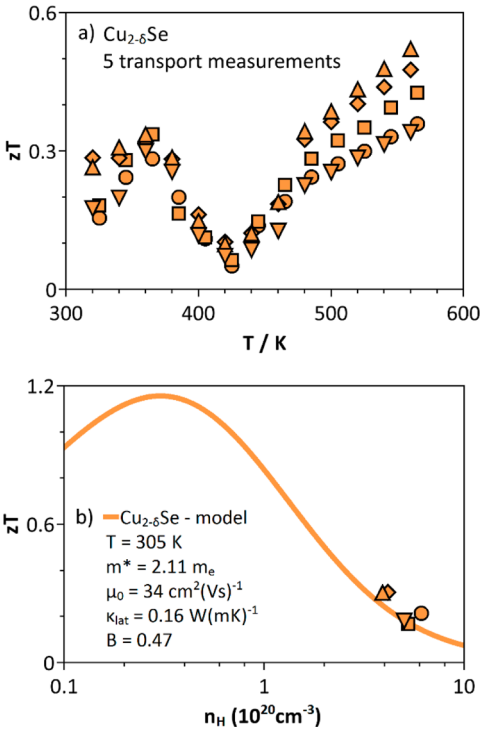

Figure 4. (a) Temperature dependence of the figure of merit zT of different copper selenide samples with a nominal composition of $Cu_{2-\delta}Se$, showing the spread of values due to the intrinsic Cu deficiency. (b) Single parabolic band model of the transport data leading to estimates of the effective mass m^*, the mobility parameter μ_0, and the quality factor B allowing a prediction of the thermoelectric figure of merit zT for different carrier concentrations. The model assumes that acoustic phonon scattering limits the carrier mobility. Reducing the hole carrier concentration in $Cu_{2-\delta}Se$ by 1 order of magnitude is predicted to result in a maximum zT of 1.16 at 305 K.

related to the intrinsic Cu deficiency δ in $Cu_{2-\delta}Se$ and the resulting changes in the Hall carrier concentrations. The actual stoichiometry of our Cu_2Se sample is about $Cu_{1.982}Se$ based on its transport properties in Figure 5. A larger δ ultimately leaves holes h^+ as carriers. The individual components of the figure of merit, Seebeck coefficient, resistivity, and thermal conductivity of one representative $Cu_{2-\delta}Se$ sample can be found in Figure 5. While the Cu vacancy in $Cu_{2-\delta}Se$ is of intrinsic nature, the holes behave extrinsically, and a single parabolic band model can be applied to analyze the transport and predict the optimum carrier densities for a maximum figure of merit.[38,39] The resulting prediction of zT versus Hall carrier concentration is shown in Figure 4b. Copper selenide is predicted to reach a maximum zT of 1.16 at 305 K with a quality factor B of 0.47 (eq 12). This value is greater than the state-of-the-art zT value for bulk materials at room temperature, which is around 1.1 achieved in $Bi_{2-x}Sb_xTe_3$.[40,41] The large zT value is a result of a relatively high weighed mobility ($\mu_0 m^{*3/2}$) of around 100 $cm^2(Vs)^{-1}$, which is comparable to the values found for PbTe and PbSe,[2] in combination with a very low lattice thermal conductivity of 0.16 $W(Km)^{-1}$. The lattice thermal conductivity was obtained using the Wiedemann–Franz law and calculated Lorenz numbers, and is much lower than typical lattice thermal conductivities of 1 $W(Km)^{-1}$ found in thermoelectric materials and possibly a result of the low symmetry crystal structure and high Cu disorder in $Cu_{2-\delta}Se$ at room temperature, which transitions into a molten Cu sublattice at high temperatures. These mechanisms are also responsible for the lattice thermal conductivity of ~0.22 $W(Km)^{-1}$ observed in Cu_7PSe_6, another superionic Cu^+ conductor.[7]

In the case of $Cu_{2-\delta}Se$, the lattice thermal conductivity of 0.16 $W(Km)^{-1}$ has to be regarded as a lower limit of κ_{lat} since it has been calculated within the single parabolic band model under the assumption that acoustic phonon scattering limits the charge carrier mobility. Differences in band structure and carrier scattering assumptions tend to lead to an overestimation of the Lorenz number and underestimation of the lattice thermal conductivities.[42] The temperature dependence of the lattice thermal conductivity below the phase transition as well as a calculation of the glass limit for the lattice thermal conductivity can be found in the Supporting Information. Modeling the thermoelectric transport and predicting the optimum carrier density have proven to be powerful tools in thermoelectrics.[43−46] Figure 4b shows that the samples of copper selenide intrinsically have a Hall carrier concentration of $4-7 \times 10^{20}$ carriers per cm^3, much greater than the optimum value of 3×10^{19} cm^{-3}. Doping this material with an electron donor should reduce the amount of holes in $Cu_{2-\delta}Se$ and therefore lower the carrier concentrations into a range of much higher figures of merit.

Thermoelectric Transport Properties in $Cu_{2-y}Se_{1-x}Br_x$. Since copper selenide is intrinsically a material with extrinsic p-type behavior, an n-type dopant (or electron donor) will be needed. A possible candidate is Br as substituent on the Se site to form $Cu_{2-y}Se_{1-x}Br_x$. Bromine has been shown to be a very effective n-type dopant in PbTe and PbSe thermoelectrics.[47,48] Copper selenide has been doped with iodine before, but this did not create an appreciable change in the room-temperature zT, and no Hall carrier concentrations were reported.[32,49] Measured transport properties of $Cu_{2-y}Se_{1-x}Br_x$ are shown in Figure 5. Comparing the transport of an undoped material (x = 0.0) with a large hole carrier concentration with the data for doped samples, it is clear that substituting Br for Se has the desired effect of reducing the carrier concentrations. The Seebeck coefficient and Hall carrier concentrations are all positive, indicating holes as the majority carriers in this system. The Hall carrier concentration n_H of the holes decreases as the amount of Br increases. The resistivity ρ and the Seebeck coefficient S both increase as x increases. The samples with x greater than zero all have markedly lower thermal conductivity than $Cu_{2-\delta}Se$ due to the reduced electronic contribution via the Wiedemann–Franz law.

Defect Formation Mechanism and Compensating Defects. While the substitution of Br for Se clearly decreases the Hall carrier concentrations of the holes, the actual changes are lower than expected. The doping efficiency of Br, calculated with respect to the high carrier concentration of the undoped $Cu_{2-\delta}Se$ is below 100% (Figure 6a). A table of the expected and measured carrier concentrations as well as the doping efficiencies can be found in Table S5. While Br usually shows high doping efficiencies,[50] low doping efficiencies in thermoelectric materials are not uncommon and often occur visibly in conjunction with phase segregations due to the Fermi level moving deeper into the band.[36,44,45] In this case, however, no secondary phases can be detected by powder X-ray diffraction or XPS. Furthermore, while usually the direction for doping is to move the Fermi level deeper into a band, i.e., increasing the carrier concentration, in this case the substitution aims at moving the Fermi level toward the band edge in an attempt to decrease the amount of carriers present. As seen in Figure 3,

DOI: 10.1021/acs.chemmater.5b02405
Chem. Mater. 2015, 27, 7018−7027

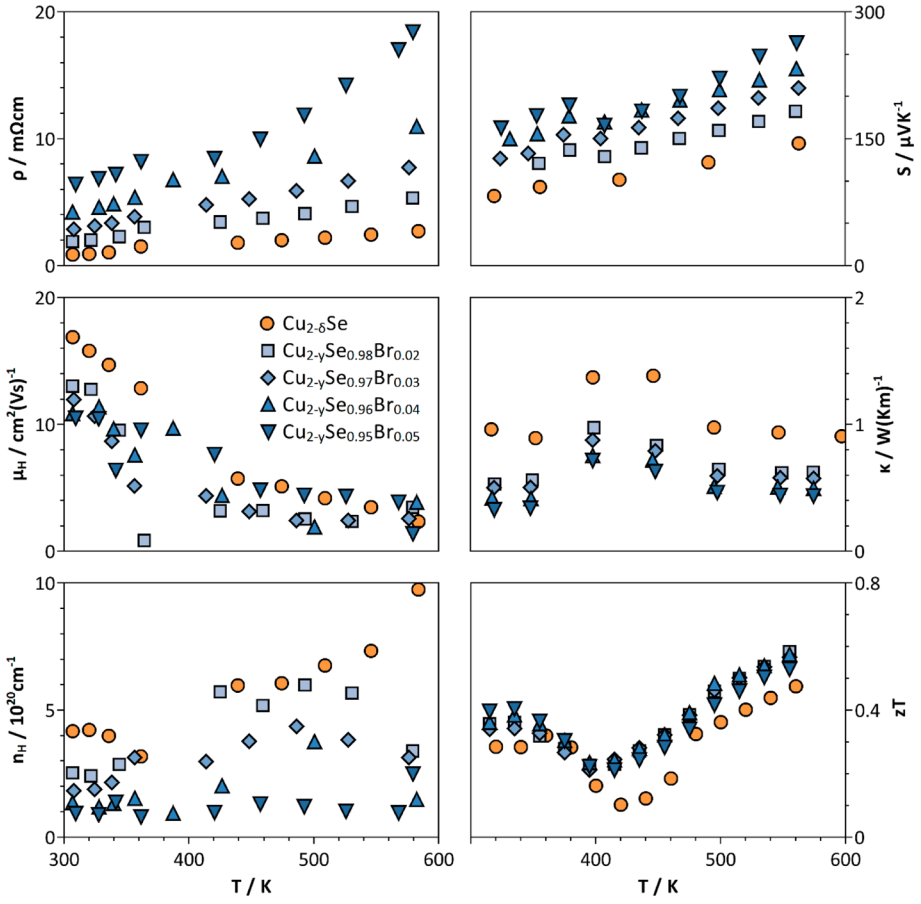

Figure 5. Temperature dependence of the thermoelectric transport properties of different bromine doped copper selenide samples $Cu_{2-y}Se_{1-x}Br_x$ with x = 0.00 (orange circles), 0.02 (blue squares), 0.03 (blue diamonds), 0.04 (blue upward triangles), and 0.05 (blue downward triangles). Bromine works as an n-type dopant in copper selenide. With increasing amounts of bromide ions, the electrical resistivity ρ and the Seebeck coefficient S increase over the investigated temperature regime due to the decreasing hole carrier concentration n_H. The total thermal conductivity decreases as well as a result of the reduced electronic contribution. Note that the Hall mobility μ_H decreases with decreasing Hall carrier concentration, and the zT values of the doped samples only increase slightly.

with increasing amounts of Br the amount of Cu in the samples decreases. Starting from the intrinsic material $Cu_{2-\delta}Se$, the synthesis does not result in a stoichiometric Cu_2Se but leads to $Cu_{2-\delta}Se$ with an excess amount of metallic copper after the synthesis (eq 1). Even though this excess amount of copper has been removed from the reaction product before hot-pressing, it can be regarded as phase segregation (eq 1). The intrinsic, Cu-defective $Cu_{2-\delta}Se$ can be expressed in the Kröger-Vink notation (eq 2),[51] showing that the copper vacancy V'_{Cu} acts as an acceptor and introduces one hole $\delta h^{\bullet}$ per copper vacancy. Note that for simplicity, in eqs 3 and 5 the reaction is written using the atomic elements, not the actual synthetic reaction with CuBr. Starting from the intrinsic material $Cu_{2-\delta}Se$, the synthesis does not result in a stoichiometric Cu_2Se but leads to $Cu_{2-\delta}Se$ with an excess amount of metallic copper after the synthesis (eq 1). Even though this excess amount of copper has been removed from the reaction product before hot-pressing, it can be regarded as phase segregation (eq 1). The intrinsic, Cu-defective $Cu_{2-\delta}Se$ can be expressed in the Kröger-Vink notation (eq 2),[51] showing that the copper vacancy V'_{Cu} acts as an acceptor and introduces one hole $\delta h^{\bullet}$ per copper vacancy. Note that for simplicity, in eqs 3 and 5 the reaction is written using the atomic elements, not the actual synthetic reaction with CuBr.

$$Cu_2Se \rightarrow Cu_{2-\delta}Se + \delta Cu \quad (1)$$

$$Cu_{2-\delta}Se = 2Cu^{\times}_{Cu} + Se^{\times}_{Se} + \delta V'_{Cu} + \delta h^{\bullet} \quad (2)$$

N-type doping with Br^- should lead to a material with composition $Cu_2Se_{1-x}Br_x$ (eq 4), if there were no Cu vacancy formation involved at all, leading to electrons due to the donor Br on the Se site $Br^{\bullet}_{Se}$:

$$2Cu + (1-x)Se + xBr \rightarrow Cu_2Se_{1-x}Br_x \quad (3)$$

$$Cu_2Se_{1-x}Br_x = 2Cu^{\times}_{Cu} + (1-x)Se^{\times}_{Se} + xBr^{\bullet}_{Se} + xe' \quad (4)$$

However, a Cu vacancy mechanism is involved (eqs 5 and 6) where the resulting composition is $Cu_{2-y}Se_{1-x}Br_x$ with y depending on the starting value of δ and x. Equation 6) shows in defect notation how the electrons, created by Br donors $Br^{\bullet}_{Se}$ are partially compensated by the holes resulting from Cu vacancy formation.

$$2Cu + (1-x)Se + xBr \rightarrow Cu_{2-y}Se_{1-x}Br_x + yCu \quad (5)$$

$$Cu_{2-y}Se_{1-x}Br_x = 2Cu^{\times}_{Cu} + yV'_{Cu} + (1-x)Se^{\times}_{Se} + xBr^{\bullet}_{Se} + xe' + yh^{\bullet} \quad (6)$$

Comparing the compositions in Figure 3, it seems that the material becomes slightly more Cu deficient with ~0.5 Cu

DOI: 10.1021/acs.chemmater.5b02405
Chem. Mater. 2015, 27, 7018−7027

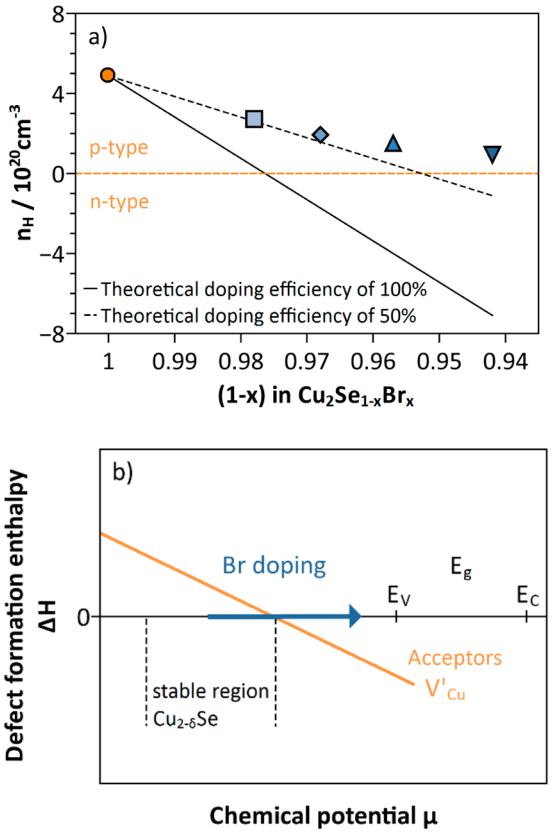

Figure 6. (a) Doping efficiency of Br in $Cu_{2-y}Se_{1-x}Br_x$. The measured Hall carrier concentration is higher than the expected carrier concentration, calculated for one electron introduced per bromide ion (Table S5). (b) Schematic defect formation enthalpy for $Cu_{2-y}Se_{1-x}Br_x$. Shifting the Fermi level to higher energies with increasing Br content x leads to a decreasing (more negative) formation enthalpy of Cu vacancies. The intrinsic defect chemistry leads to the observed lower doping efficiency of 50%, where each bromide ion creates half a killer vacancy of Cu.

vacancies per Br introduced into the system. While bromine introduces an electron into the system, the resulting 0.5 Cu vacancies will introduce half a hole in comparison, leading to a doping efficiency of 50%. This can indeed be observed for lower values of x, whereas at higher doping content the change in the carrier concentration flattens out (Figure 6a). The drop in efficiency can be related to segregation (or nonreaction) of CuBr, which should introduce even more holes. As the samples with larger synthetic amount of Br ($x > 0.7$) showed CuBr as secondary phases, this mechanism seems reasonable. While vacancy formation has already been shown to have an important effect on the carrier concentration in AZn_2Sb_2 Zintl phases,[52,53] the compositional data and the resulting carrier concentrations clearly show the influence of Cu vacancy formation as a compensating defect in this material. Zunger has provided a model to understand the influence of defects on the Fermi level in semiconductors.[54] For instance, when an electron producing dopant (donor, Br^- in this case) becomes incorporated in a solid, it raises the Fermi level. When the Fermi level is raised further into the conduction band, at some point the defect formation enthalpy of acceptor defects becomes negative, and acceptor defects such as cation vacancies or interstitials are created. These acceptor defects act as "killer defects," effectively pinning the Fermi level to a maximum.[54] In the case of a p-type material, hole doping (introducing an acceptor) will shift the Fermi level deeper into the valence band, and the competing mechanism is either the formation of anion vacancies or cation interstitials, which will also result in the pinning of the Fermi level via killer defects. In the case of $Cu_{2-y}Se_{1-x}Br_x$, the occurrence of copper vacancies V_{Cu}^- as "killer defects" occurs when moving the Fermi level closer to the valence band edge and not further into the conduction band. The intrinsic material $Cu_{2-\delta}Se$ already is deficient in Cu, i.e., $\delta > 0$, due to entropic reasons leading to a temperature and intrinsic defect enthalpy dependence of δ. With increasing Br content, the defect formation enthalpy for copper vacancies V'_{Cu} becomes negative (Figure 6b, orange line). This response can also be considered along the lines of Le Chatelier's principle because adding Br alters a system which has an equilibrium Cu defect concentration and Fermi level. The system then adjusts to partially counteract the raising of the Fermi level caused by bromine substitutional defects by increasing the concentration of the compensating copper vacancy defect. In other words, the dependence of the defect formation enthalpy for V'_{Cu} in $Cu_{2-\delta}Se$ is shifted to values where any increase in the Fermi level will introduce more Cu vacancies, which ultimately act as compensating defects in the valence band.

Charge Carrier Scattering Mechanism. While the parabolic band model in Figure 4b predicts an improvement of the figure of merit at room temperature, the measured zT values do not exceed unity, and those at high temperatures are only slightly greater than the zT values of $Cu_{2-\delta}Se$. This is in accordance with the findings for iodine doped $Cu_{2-\delta}Se$.[32] To understand why doping with Br did not result in the predicted high zT values, we look at the results of the SPB model for data at 305 K, shown in Figure 7. All parameters for the model at 305 K and a full transport model and description for the temperature of 550 K can be found in the Supporting Information. Figure 7b shows a prediction of how S should change with n_H in copper selenide using Pisarenko relationships. Orange symbols denote $Cu_{2-\delta}Se$, and blue symbols denote $Cu_{2-y}Se_{1-x}Br_x$. Each material was analyzed separately. The effective masses for each material are within 2% of one another, and it appears that Br does not change the curvature and hence the density of states effective mass of the valence band of $Cu_{2-\delta}Se$. The values for the lattice thermal conductivity (Figure 7c) are also the same within the measurement uncertainty, 0.16 and 0.20 W $(Km)^{-1}$ for $Cu_{2-\delta}Se$ and $Cu_{2-y}Se_{1-x}Br_x$, respectively. The most striking difference between the two materials is the change in the mobility parameter (Figure 7a). Copper selenide has a mobility parameter of 34 $cm^2(Vs)^{-1}$, but $Cu_{2-y}Se_{1-x}Br_x$ has a mobility parameter of only 17 $cm^2(Vs)^{-1}$. It appears that adding Br drastically reduces the mobility of the holes in the valence band. In a material influenced by a single parabolic band and with acoustic phonons as the main scatterers of electrons, the Hall mobility should decrease with increasing Hall carrier concentrations.[55,56] The Hall mobility data for $Cu_{2-y}Se_{1-x}Br_x$ in Figure 7a exhibit a slight upward trend with Hall carrier concentration. In order to understand this unexpected behavior, we need to incorporate another scattering mechanism to understand this contradiction of our assumptions.

The scattering mechanism for electrons and holes is represented by the scattering relaxation time:[55,56]

$$\tau = \tau_0 \epsilon^{\lambda - 1/2} \quad (7)$$

where ϵ is the dimensionless charge carrier energy. Each scattering mechanism has a characteristic equation for τ_0 and

DOI: 10.1021/acs.chemmater.5b02405
Chem. Mater. 2015, 27, 7018−7027

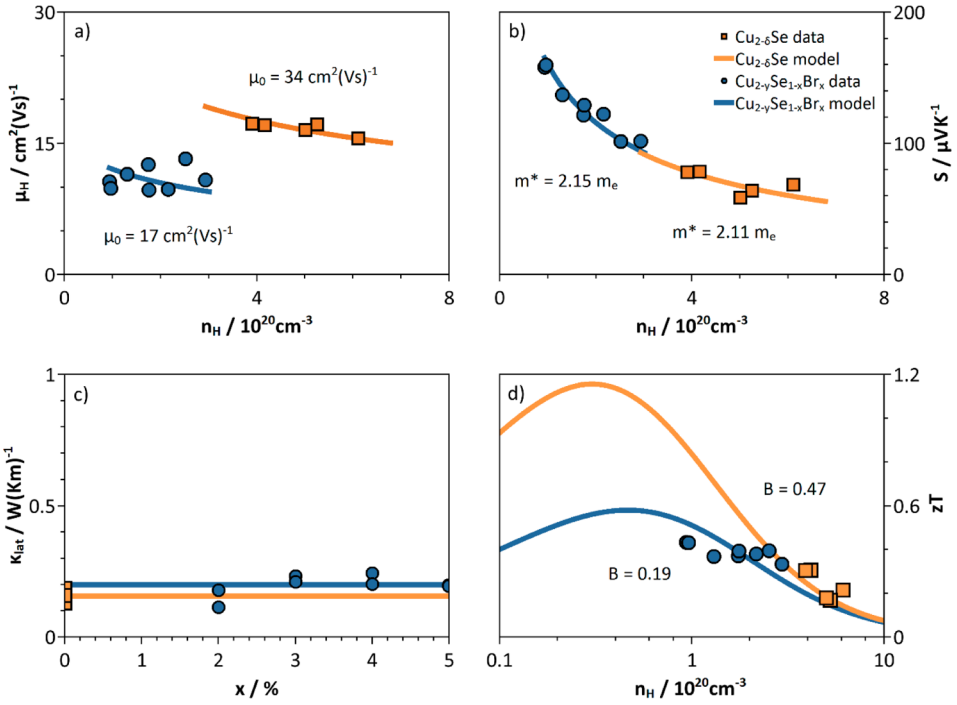

Figure 7. Results for the SPB model for $Cu_{2-\delta}Se$ and $Cu_{2-y}Se_{1-x}Br_x$ at 305 K under the assumption of acoustic phonon scattering. The Pisarenko relationship (a) predicts how S changes with n_H in copper selenide. Orange squares denote $Cu_{2-\delta}Se$, and blue circles denote $Cu_{2-y}Se_{1-x}Br_x$. The effective masses are basically identical, and Br does not have a huge influence on the curvature of the valence band of $Cu_{2-\delta}Se$. However, the n_H dependence of the mobility parameter does not represent the expected trends (modeled lines) for acoustic phonon scattering (a) as n_H increases slightly with μ_H for $Cu_{2-y}Se_{1-x}Br_x$.

value of λ. When one scattering mechanism does not dominate scattering in the material, multiple scattering rates must be taken into account. Each scattering rate is equal to $1/\tau_i$, where τ_i is the relaxation time for a particular scattering mechanism. The scattering rates are treated like resistors in series, so the total scattering rate $1/\tau$ is equal to the sum of the individual scattering rates $1/\tau_i$ (Matthiessen's rule). The relaxation time for acoustic phonon scattering is given by[57,58]

$$\tau_{ac} = \frac{\pi\hbar^4 v_l^2 d}{\sqrt{2}\Xi^2 (m\cdot kT)^{3/2}} \epsilon^{-1/2} \tag{8}$$

where Ξ is the deformation potential, v_l is the longitudinal speed of sound, and d is the density. Since two kinds of atoms occupy the Se site (Se and Br), it is logical to include an alloy scattering mechanism. The relaxation time for alloy scattering is[59]

$$\tau_{\text{alloy}} = \frac{8\hbar^4}{3\sqrt{2}\,V_{\text{atom}} x(1-x) U^2 m^{*3/2} (kT)^{1/2}} \epsilon^{-1/2} \tag{9}$$

with $V_{atom} = M(nNAd)^{-1}$ the molecular weight is M, n is the number of atoms per formula unit, d is the density, and N_A is Avogadro's constant. U is the alloy scattering potential, which is similar to the deformation potential Ξ in that it describes the way the scattering mechanism changes the energy states of the charge carriers. x is the fraction of substituted atoms. The densities and respective speeds of sounds for the different compositions can be found in Table S2. As stated above, the total relaxation time τ is related to the total scattering rate $1/\tau$:

$$\tau^{-1} = \tau_{ac}^{-1} + \tau_{\text{alloy}}^{-1} \tag{10}$$

The scattering mechanism determines the parameter λ, which in turn determines the order of the Fermi integrals used to calculate the transport properties. Since τ_{ac} and τ_{alloy} have the same dependence on λ ($\lambda = 0$), including alloy scattering into the modeling does not change the order of the Fermi integrals, and μ_0 can be modeled separately. Using τ and the effective mass m^*, the mobility parameter μ_0 can be calculated via

$$\mu_0 = e\tau/m^* \tag{11}$$

Applying the combined acoustic phonon/alloy scattering model to values of μ_0 computed for each value of x with the deformation potential Ξ and the alloy scattering potential U as free parameters, we obtain a deformation potential of 5.8 eV and an alloy scattering potential of 1.1 eV. The deformation potential obtained for $Cu_{2-y}Se_{1-x}Br_x$ is equal to that obtained for $Cu_{2-\delta}Se$, and alloy scattering potentials around 1.1 can be found in several other solid solutions like n-type $PbSe_{1-x}Te_x$, $Cd_{1-x}Zn_xTe$, or $Al_{1-x}Ga_xAs$.[60−62] The Hall mobility versus Hall carrier concentration curve accounting for acoustic phonon and alloy scattering is shown in Figure 8, showing that due to increased alloy scattering via Br introduction, a reduction of the mobility can be observed. This reduction in μ_0 in the Br-doped samples due to alloy scattering reduces the quality factor B (eq 12) of $Cu_{2-\delta}Se$ from 0.47 to 0.19 (Figure 7d). The quality factor B is a measure of the maximum zT at a given temperature and is given by[63,64]

$$B = \frac{8\pi e}{3}\left(\frac{k_B}{e}\right)^2\left(\frac{2m_e k_B}{h^2}\right)^{3/2} \frac{\mu_0 (m^*/m_e)^{3/2} T^{5/2}}{\kappa_{\text{lat}}} \tag{12}$$

While Br acts as an electron donor, i.e., it reduces the hole carrier concentration and increases the Seebeck coefficient, the additional scattering from the dissimilar atoms on the anion site

DOI: 10.1021/acs.chemmater.5b02405
Chem. Mater. 2015, 27, 7018−7027

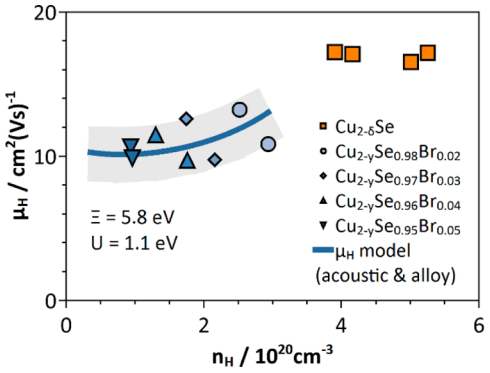

Figure 8. Hall mobility versus Hall carrier concentration at 305 K for the undoped (orange squares) and doped (blue) $Cu_{2-y}Se_{1-x}Br_x$ samples. Two pellets for each composition with $x > 0$ were measured. The blue line represents the model for the Hall mobility including acoustic phonon and alloy scattering. An error in mobility of 10% is represented by the thick gray line. Alloy scattering can explain decreasing mobility for the doped samples using a deformation potential of 5.8 eV and an alloy scattering potential of 1.1 eV.

reduces the maximum possible zT to 0.6. Figure 7d shows how the figure of merit's increase with decreasing carrier concentration slows down due to a changing mobility. Similar effects have been observed in lead chalcogenides and has recently systematically been investigated by Wang et al.,[50] where it was shown that the mobility reduction due to chemical substitution on a certain sublattice depends on its contribution to the charge conducting band. The huge degree of mobility reduction observed in $Cu_{2-y}Se_{1-x}Br_x$ indicates a high contribution of the anion atomic orbitals to the valence band states close to the Fermi energy, which strongly influences the hole mobility. Because of the complex crystal structure at room temperature, band structure calculations are only available for high temperature modification. However, the available calculations show a large contribution of the anion sublattice to the valence band at high temperature.[65] It should be noted, however, that another possible scattering mechanism could be ionized impurity scattering, which would express itself as an increase of the Hall carrier mobility at higher carrier concentrations as well, due to screening effects.[66] One might think that ionized impurity scattering would play a role in $Cu_{2-y}Se_{1-x}Br_x$ due to the charge differences in Se^{2-} and Br^-, and an upward trend of μ_H with n_H can indeed be seen. However, applying a combined acoustic phonon and ionized impurity scattering model to the data at 305 K indicates that ionized impurity scattering is not the predominant scattering mechanism in heavily doped $Cu_{2-y}Se_{1-x}Br_x$. Therefore, the electronic conduction can be sufficiently described by a combined acoustic phonon/alloy scattering model for high carrier concentrations, which has been successfully utilized to describe the electrical transport of other heavily doped systems like PbTe.[50] This is encouraging because it suggests that doping with something other than Br may not affect the mobility parameter possibly leading to larger quality factors and figures of merit, whereas ionized impurity scattering implies that any dopant would reduce μ_0 and therefore reduce the maximum potential zT. In this context, an investigation of corresponding cation doped copper selenides would be very interesting as the reduction of the mobility could be much less pronounced here due to a smaller contribution of the cation sublattice to the valence band. To our knowledge, cation doped copper selenide has never been successfully synthesized, which might be due to the different chemistries of copper compared to that of the other 3d elements. Our own doping attempts with nickel and zinc led to the formation of nickel and zinc selenide (NiAs structure) even for very low substitution grades. However, as Zunger has pointed out designing growth and synthesis conditions may be effective in obtaining the predicted high figure of merit without detrimental effects on the carrier mobility.[54]

SUMMARY

We have demonstrated that $Cu_{2-\delta}Se$ has the potential to be a high-performance thermoelectric material at room temperature if the intrinsic heavily doped character can be altered. Using bromine as an electron donor, we have successfully shown that it is possible to reduce the hole concentration in copper selenide. Exploring the different possible scattering mechanisms for holes in this material showed that doping on the chemical site, which mostly contributes to the valence band, leads to enhanced alloy scattering and a reduced mobility when doping with bromine. While it shows that Br is not an ideal dopant to achieve the predicted thermoelectric performance in $Cu_{2-\delta}Se$, different strategies for further improvement should indeed be possible because ionized impurity scattering does not play a role here. Furthermore, we have shown the reduced doping efficiency of Br by increasing amounts of copper vacancies due to Br substitution on the Se site. The interesting defect chemistry of $Cu_{2-\delta}Se$ shows, for the first time, that compensating defects and an effective pinning of the Fermi level can be achieved when shifting the chemical potential toward the valence band edge as opposed to deeper into the conduction band. This work shows the need to fully understand the underlying scattering mechanisms and the crystal and defect chemistry of a material in order to achieve high figure of merit thermoelectrics.

ASSOCIATED CONTENT

Supporting Information

The Supporting Information is available free of charge on the ACS Publications website at DOI: 10.1021/acs.chemmater.5b02405.

Exemplary X-ray powder diffraction data of $Cu_{2-\delta}Se$ with corresponding Pawley fits; X-ray powder diffraction data of all synthesized $Cu_{2-y}Se_{1-x}Br_x$ powders with x up to 0.1; additional information about the XPS, XRF, and ICP-MS measurements, including XRF spectra, detailed description of the sample preparation for the ICP-MS measurement with operating parameters and the results for the relative compositions, which were used for Figure 3; results of additional measurements required for the analysis of the transport data like speed of sound and densities of the investigated samples; SPB results for $Cu_{2-y}Se_{1-x}Br_x$ at higher temperatures; measured and theoretical charge carrier concentrations, which were used for the determination of the doping efficiency in Figure 6; temperature dependences of the lattice thermal conductivity κ_{lat} in $Cu_{2-y}Se_{1-x}Br_x$ as well as the glassy limit of the lattice thermal conductivity κ_{min}; Pisarenko plot comparing a combined acoustic and alloy scattering model with a combined acoustic and ionized impurity scattering model (PDF)

DOI: 10.1021/acs.chemmater.5b02405
Chem. Mater. 2015, 27, 7018−7027

AUTHOR INFORMATION

Corresponding Authors

*(G.J.S.) E-mail: jeff.snyder@northwestern.edu.
*(W.T.) E-mail: tremel@uni-mainz.de.

Author Contributions

#T.W.D. and K.S.W. contributed equally to this work.

Notes

The authors declare no competing financial interest.

ACKNOWLEDGMENTS

We acknowledge support from the DFG priority program SPP1386 "Nanostructured Thermoelectrics". W.G.Z. and G.J.S. acknowledge the EFRC Solid-State Solar-Thermal Energy Conversion Center (S3TEC) award number DE-SC0001299. This work made use of the J. B. Cohen X-ray Diffraction Facility supported by the MRSEC program of the National Science Foundation (DMR-1121262) at the Materials Research Center of Northwestern University. The XPS work was performed in the Keck-II facility of NUANCE Center at Northwestern University. The NUANCE Center is supported by the International Institute for Nanotechnology, MRSEC (NSF DMR-1121262), the Keck Foundation, the State of Illinois, and Northwestern University. T.W.D. and G.J.S. are grateful for the support of the United States Air Force Office of Scientific Research. We thank Riley Hanus for the collection of atom probe data. We also acknowledge Afrora Lulaj and Karoline Herget for their assistance in sample preparation.

REFERENCES

(1) Bell, L. E. Cooling, heating, generating power, and recovering waste heat with thermoelectric systems. *Science* **2008**, *321*, 1457.

(2) Slack, G. A. in *CRC Handbook of Thermoelectrics*; Rowe, D. M., Ed.; CRC Press: Boca Raton, FL, 1995.

(3) Pei, Y.; Shi, X.; LaLonde, A.; Wang, H.; Chen, L.; Snyder, G. J. Convergence of electronic bands for high performance bulk thermoelectrics. *Nature* **2011**, *473*, 66.

(4) Sorokin, G. P.; Papshev, Y. M.; Oush, P. T. Photoconductivity of Cu_2S, Cu_2Se, and Cu_2Te. *Sov. Phys. Solid State* **1966**, *7*, 1810.

(5) Liu, H.; Shi, X.; Xu, F.; Zhang, L.; Zhang, W.; Chen, L.; Li, Q.; Uher, C.; Day, T.; Snyder, G. J. Copper ion liquid-like thermoelectrics. *Nat. Mater.* **2012**, *11*, 422.

(6) Brown, D. R.; Day, T.; Borup, K. a.; Christensen, S.; Iversen, B. B.; Snyder, G. J. Phase transition enhanced thermoelectric figure-of-merit in copper chalcogenides. *APL Mater.* **2013**, *1*, 052107.

(7) Weldert, K. S.; Zeier, W. G.; Day, T. W.; Panthöfer, M.; Snyder, G. J.; Tremel, W. Thermoelectric transport in Cu_7PSe_6 with high copper ionic mobility. *J. Am. Chem. Soc.* **2014**, *136*, 12035.

(8) Day, T.; Drymiotis, F.; Zhang, T.; Rhodes, D.; Shi, X.; Chen, L.; Snyder, G. J. Evaluating the potential for high thermoelectric efficiency of silver selenide. *J. Mater. Chem. C* **2013**, *1*, 7568.

(9) Ferhat, M.; Nagao, J. Thermoelectric and transport properties of β-Ag2Se compounds. *J. Appl. Phys.* **2000**, *88*, 813.

(10) Drymiotis, F.; Day, T. W.; Brown, D. R.; Heinz, N. a.; Jeffrey Snyder, G. Enhanced thermoelectric performance in the very low thermal conductivity $Ag_2Se_{0.5}Te_{0.5}$. *Appl. Phys. Lett.* **2013**, *103*, 143906.

(11) Ishiwata, S.; Shiomi, Y.; Lee, J. S.; Bahramy, M. S.; Suzuki, T.; Uchida, M.; Arita, R.; Taguchi, Y.; Tokura, Y. Extremely high electron mobility in a phonon-glass semimetal. *Nat. Mater.* **2013**, *12*, 512.

(12) Hong, A. J.; Li, L.; Zhu, H. X.; Zhou, X. H.; He, Q. Y.; Liu, W. S.; Yan, Z. B.; Liu, J. M.; Ren, Z. F. Anomalous transport and thermoelectric performances of CuAgSe compounds. *Solid State Ionics* **2014**, *261*, 21.

(13) Zeier, W. G.; Heinrich, C. P.; Day, T.; Panithipongwut, C.; Kieslich, G.; Brunklaus, G.; Snyder, G. J.; Tremel, W. Bond strength dependent superionic phase transformation in the solid solution series $Cu_2ZnGeSe_{4-x}S_x$. *J. Mater. Chem. A* **2014**, *2*, 1790.

(14) Zhang, J.; Liu, R.; Cheng, N.; Zhang, Y.; Yang, J.; Uher, C.; Shi, X.; Chen, L.; Zhang, W. High-Performance Pseudocubic Thermoelectric Materials from Non-cubic Chalcopyrite Compounds. *Adv. Mater.* **2014**, *26*, 3848.

(15) Zeier, W. G.; Zhu, H.; Gibbs, Z. M.; Ceder, G.; Tremel, W.; Snyder, G. J. Band convergence in the non-cubic chalcopyrite compounds Cu_2MGeSe_4. *J. Mater. Chem. C* **2014**, *2*, 10189.

(16) Brown, D. R.; Day, T.; Caillat, T.; Snyder, G. J. Chemical stability of $(Ag,Cu)_2Se$: a historical overview. *J. Electron. Mater.* **2013**, *42*, 2014.

(17) Heyding, R. D. The copper selenium system. *Can. J. Chem.* **1966**, *44*, 1233.

(18) Ishikawa, T.; Miyatani, S. Electronic and Ionic Conduction in $Cu_{2-\delta}Se$, $Cu_{2-\delta}S$ and $Cu_{2-\delta}(Se,S)$. *J. Phys. Soc. Jpn.* **1977**, *42*, 159−167.

(19) LaLonde, A. D.; Ikeda, T.; Snyder, G. J. Rapid consolidation of powdered materials by induction hot pressing. *Rev. Sci. Instrum.* **2011**, *82*, 025104.

(20) Coelho, A. *TOPAS-Academic V5*, Coelho Software: Brisbane, Australia, 2012.

(21) Day, T. W.; Borup, K. a.; Zhang, T.; Drymiotis, F.; Brown, D. R.; Shi, X.; Chen, L.; Iversen, B. B.; Snyder, G. J. High-temperature thermoelectric properties of $Cu_{1.97}Ag_{0.03}Se_{1+y}$. *Mater. Renew. Sustain. Energy* **2014**, *3*, 26.

(22) Horvatic, M.; Vucic, Z. DC ionic conductivity measurements on the mixed conductor $Cu_{2-x}Se$. *Solid State Ionics* **1984**, *13*, 117.

(23) Chatov, V. A.; Iorga, T. P.; Inglizyan, P. N. Ionic conduction and diffusion of copper in copper selenide. *Sov. Phys. Semicond.* **1980**, *14*, 474.

(24) Yamamoto, K.; Kashida, S. X-ray study of the average structures of Cu_2Se and $Cu_{1.8}S$ in the room temperature and the high temperature phases. *J. Solid State Chem.* **1991**, *93*, 202.

(25) Kashida, S.; Akai, J. X-ray diffraction and electron microscopy studies of the room-temperature structure of Cu_2Se. *J. Phys. C: Solid State Phys.* **1988**, *21*, 5329.

(26) Moulder, J. F.; Stickle, W. F.; Sobol, P. E.; Bomben, K. D. *Handbook of X-ray Photoelectron Spectroscopy*; Physical Electronics Inc.: Eden Prairie, MN, 1995.

(27) Borchert, W. Gitterumwandlungen im System $Cu_{2-x}Se$. *Z. Kristallogr.* **1954**, *106*, 5.

(28) Stevels, A. L. N.; Jellinek, F. Phase transitions in copper chalcogenides: I. The copper-selenium system. *Rec. Trav. Chim. Pays-Bas* **1971**, *90*, 273.

(29) Murray, R. M.; Heyding, R. D. The Copper-Selenium System at Temperatures to 850 K and Pressures to 50 Kbar. *Can. J. Chem.* **1975**, *53*, 878.

(30) Vučić, Z.; Milat, O.; Horvatić, V.; Ogorelec, Z. Composition-induced phase-transition splitting in cuprous selenide. *Phys. Rev. B: Condens. Matter Mater. Phys.* **1981**, *24*, 5398.

(31) Skomorokhov, A. N.; Trots, D. M.; Knapp, M.; Bickulova, N. N.; Fuess, H. Structural behaviour of β-$Cu_{2-\delta}Se$ (δ = 0, 0.15, 0.25) in dependence on temperature studied by synchrotron powder diffraction. *J. Alloys Compd.* **2006**, *421*, 64.

(32) Zhao, L. L.; Wang, X. L.; Wang, J. Y.; Cheng, Z. X.; Dou, S. X.; Wang, J.; Liu, L. Q. Superior intrinsic thermoelectric performance with zT of 1.8 in single-crystal and melt-quenched highly dense $Cu_{2-x}Se$ bulks. *Sci. Rep.* **2015**, *5*, 7671.

(33) Zhao, L.; Wang, X.; Yun, F. F.; Wang, J.; Cheng, Z.; Dou, S.; Wang, J.; Snyder, G. J. The Effects of Te^{2-} and I^- Substitutions on the Electronic Structures, Thermoelectric Performance, and Hardness in Melt-Quenched Highly Dense $Cu_{2-x}Se$. *Adv. Electron. Mater.* **2015**, *1*, 1400015.

(34) Liu, Y.; Yang, J.; Gu, E.; Cao, T.; Su, Z.; Jiang, L.; Yan, C.; Hao, X.; Liu, F.; Liu, Y. Colloidal synthesis and characterisation of Cu 3 SbSe 3 nanocrystals. *J. Mater. Chem. A* **2014**, *2*, 6363.

(35) Wang, W.; Zhang, L.; Chen, G.; Jiang, J.; Ding, T.; Zuo, J.; Yang, Q. $Cu_{2-x}Se$ nanooctahedra: controllable synthesis and optoelectronic properties. *CrystEngComm* **2015**, *17* (9), 1975.

DOI: 10.1021/acs.chemmater.5b02405
Chem. Mater. 2015, 27, 7018−7027

(36) Zeier, W. G.; LaLonde, A.; Gibbs, Z. M.; Heinrich, C. P.; Panthöfer, M.; Snyder, G. J.; Tremel, W. Influence of a Nano Phase Segregation on the Thermoelectric Properties of the p-Type Doped Stannite Compound $Cu_{2+x}Zn_{1-x}GeSe_4$. *J. Am. Chem. Soc.* **2012**, *134*, 7147.
(37) Day, T. W.; Zeier, W. G.; Brown, D. R.; Melot, B. C.; Snyder, G. J. Determining conductivity and mobility values of individual components in multiphase composite $Cu_{1.97}Ag_{0.03}Se$. *Appl. Phys. Lett.* **2014**, *105*, 172103.
(38) El Akkad, F.; Mansour, B.; Hendeya, T. Electrical and thermoelectric properties of Cu_2Se and Cu_2S. *Mater. Res. Bull.* **1981**, *16*, 535.
(39) May, A. F.; Snyder, G. J. In *Thermoelectrics Handbook: Thermoelectrics and Its Energy Harvesting*; Rowe, D. M., Ed.; CRC Press: Boca Raton, FL, 2012; Chapter 11.
(40) Scherrer, H.; Scherrer, S. *Thermoelectics Handbook: Macro to Nano*; CRC Press: Boca Raton, 2006; Chapter 27.
(41) Fleurial, J. P.; Gailliard, L.; Triboulet, R.; Scherrer, H.; Scherrer, S. Thermal properties of high quality single crystals of bismuth telluride-Part I: Experimental characterization. *J. Phys. Chem. Solids* **1988**, *49* (10), 1237.
(42) Kim, H.-S.; Gibbs, Z. M.; Tang, Y.; Wang, H.; Snyder, G. J. Characterization of Lorenz number with Seebeck coefficient measurement. *APL Mater.* **2015**, *3*, 041506.
(43) May, A.; Toberer, E.; Saramat, A.; Snyder, G. J. Characterization and analysis of thermoelectric transport in n-type $Ba_8Ga_{16-x}Ge_{30+x}$. *Phys. Rev. B: Condens. Matter Mater. Phys.* **2009**, *80*, 1.
(44) Zevalkink, A.; Zeier, W. G.; Pomrehn, G.; Schechtel, E.; Tremel, W.; Snyder, G. J. Thermoelectric properties of Sr_3GaSb_3 − a chain-forming Zintl compound. *Energy Environ. Sci.* **2012**, *5*, 9121.
(45) Zevalkink, A.; Toberer, E. S.; Zeier, W. G.; Flage-Larsen, E.; Snyder, G. J. Ca_3AlSb_3: an inexpensive, non-toxic thermoelectric material for waste heat recovery. *Energy Environ. Sci.* **2011**, *4*, 510.
(46) Zeier, W. G.; Zevalkink, A.; Schechtel, E.; Tremel, W.; Snyder, G. J. Thermoelectric properties of Zn-doped Ca_3AlSb_3. *J. Mater. Chem.* **2012**, *22*, 9826.
(47) Pei, Y.; Wang, H.; Snyder, G. J. Band engineering of thermoelectric materials. *Adv. Mater.* **2012**, *24*, 6125.
(48) Wang, H.; Pei, Y.; LaLonde, a. D.; Snyder, G. J. Weak electron−phonon coupling contributing to high thermoelectric performance in n-type PbSe. *Proc. Natl. Acad. Sci. U. S. A.* **2012**, *109*, 9705.
(49) Liu, H.; Yuan, X.; Lu, P.; Shi, X.; Xu, F.; He, Y.; Tang, Y.; Bai, S.; Zhang, W.; Chen, L.; Lin, Y.; Shi, L.; Lin, H.; Gao, X.; Zhang, X.; Chi, H.; Uher, C. Ultrahigh Thermoelectric Performance by Electron and Phonon Critical Scattering in $Cu_2Se_{1-x}I_x$. *Adv. Mater.* **2013**, *25*, 6607.
(50) Wang, H.; Cao, X.; Takagiwa, Y.; Snyder, G. J. Higher mobility in bulk semiconductors by separating the dopants from the charge-conducting band − a case study of thermoelectric PbSe. *Mater. Horiz.* **2015**, *2*, 323.
(51) Kroeger, F. A.; Vink, H. J. Relations between the concentrations of imperfections in crystalline solids. *Solid State Phys.* **1956**, *3*, 307.
(52) Pomrehn, G. S.; Zevalkink, A.; Zeier, W. G.; Van De Walle, A.; Snyder, G. J. Defect-Controlled Electronic Properties in AZn_2Sb_2 Zintl Phases. *Angew. Chem., Int. Ed.* **2014**, *53*, 3422.
(53) Zevalkink, A.; Zeier, W. G.; Cheng, E.; Snyder, J.; Fleurial, J.-P.; Bux, S. Nonstoichiometry in the Zintl Phase $Yb_{1-\delta}Zn_2Sb_2$ as a Route to Thermoelectric Optimization. *Chem. Mater.* **2014**, *26*, 5710.
(54) Zunger, A. Practical doping principles. *Appl. Phys. Lett.* **2003**, *83*, 57.
(55) Goldsmid, H. *Applications of Thermoelectricity*; Butler & Tanner Ltd.: London, 1960.
(56) Ioffe, A. F. *Semiconductor Thermoelements and Thermoelectric Cooling*; Infosearch: London, 1957.
(57) Wilson, A. H. *The Theory of Metals*; Cambridge University Press: New York, 1958.
(58) Bardeen, J.; Shockley, W. Deformation potentials and mobilities in non-polar crystals. *Phys. Rev.* **1950**, *80*, 72.
(59) Harrison, J. W.; Hauser, J. R. Alloy scattering in ternary III-V compounds. *Phys. Rev. B* **1976**, *13*, 5347.
(60) Wang, H.; Lalonde, A. D.; Pei, Y.; Snyder, G. J. The criteria for beneficial disorder in thermoelectric solid solutions. *Adv. Funct. Mater.* **2013**, *23*, 1586.
(61) Movchan, S.; Sizov, F.; Tetyorkin, V. Photosensitive heterostructures CdTe-PbTe prepared by hot-wall technique. *Semicond. Phys., Quantum Electron. Optoelectron.* **1999**, *2*, 84.
(62) Li, W. L.; Csathy, G. A.; Tsui, D. C.; Pfeiffer, L. N.; West, K. W. Direct observation of alloy scattering of two-dimensional electrons in $Al_xGa_{1-x}As$. *Appl. Phys. Lett.* **2003**, *83*, 2832.
(63) Chasmar, R. P.; Stratton, R. The Thermoelectric Figure of Merit and its Relation to Thermoelectric Generators. *J. Electron. Control* **1959**, *7*, 52.
(64) Wang, H.; Pei, Y.; Lalonde, A. D.; Snyder, G. J. In *Springer Series in Materials Science, 182*; Koumoto, K., Mori, T., Eds.; Springer Verlag: Berlin, Germany, 2013.
(65) Rasander, M.; Bergqvist, L.; Delin, A. Density functional theory study of the electronic structure of fluorite Cu_2Se. *J. Phys.: Condens. Matter* **2013**, *25*, 125503.
(66) Chattopadhyay, D.; Queisser, H. J. Electron scattering by ionized impurities in semiconductors. *Rev. Mod. Phys.* **1981**, *53*, 745.

DOI: 10.1021/acs.chemmater.5b02405
Chem. Mater. 2015, 27, 7018−7027